

<sup>1</sup> Islandization of terrestrial protected areas

<sup>2</sup> Amy Van Scoyoc <sup>1\*</sup>, Wenjing Xu <sup>1,2\*</sup>, Carl Boettiger<sup>1</sup> and  
<sup>3</sup> Justin Brashares<sup>1</sup>

<sup>4</sup> <sup>1</sup> Department of Environmental Science, Policy, and Management  
<sup>5</sup> University of California, Berkeley Berkeley California United States.

<sup>6</sup> <sup>2</sup> Senckenberg Biodiversity and Climate Research Centre Goethe  
<sup>7</sup> University of Frankfurt Frankfurt Germany.

<sup>8</sup> Contributing authors: [avanscoyoc@berkeley.edu](mailto:avanscoyoc@berkeley.edu);  
<sup>9</sup> [wenjing.xu@senckenberg.de](mailto:wenjing.xu@senckenberg.de);

<sup>10</sup> **Abstract**

<sup>11</sup> Recent global commitments to biodiversity conservation focus on safeguarding  
<sup>12</sup> habitat connectivity to preserve landscape-scale ecological processes and the  
<sup>13</sup> capacity for adaptation to rapid global change. While many key studies have  
<sup>14</sup> quantified changes in forest cover to highlight the potential isolation of protected  
<sup>15</sup> areas via their edges, biome-wide assessments of edges at protected areas bound-  
<sup>16</sup>aries have been few to none. Here, we quantified the rate of change in edges along  
<sup>17</sup> XXXX protected area boundaries over 23-year period (2001 - 2023). We achieved  
<sup>18</sup> a comparative biome-wide global assessment by using 500m MODIS satellite  
<sup>19</sup> imagery and a pixel-based approach to compute the contrast in spectral values  
<sup>20</sup> along the 10km boundary of XXXX protected areas representing all terrestrial  
<sup>21</sup> biomes for all visible bands and several remote sensing indices. Nearly half the  
<sup>22</sup> world's protected areas showed accelerated islandization over a 23-year period  
<sup>23</sup> (2001-2023). Surprisingly, protected areas in grassland and shrubland biomes  
<sup>24</sup> showed the greatest rates of islandization over time. These findings highlight  
<sup>25</sup> the challenges and opportunities for utilizing protected areas as the backbone of  
<sup>26</sup> post-2020 initiatives for large-landscape conservation.

<sup>27</sup> **Keywords:** protected areas, islandization, habitat continuity, MODIS, geospatial  
<sup>28</sup> analysis

## **29    1 Introduction**

**30** Differences in adjacent land cover or land use—referred to as ‘edges’—can fragment  
**31** habitat and reduce landscape connectivity for plants and animals. Edge effects are  
**32** known to disrupt ecological processes such as migration and dispersal, with conse-  
**33** quences for population demography, gene flow, and long-term persistence. As a result,  
**34** maintaining landscape connectivity is a central goal of global biodiversity conservation  
**35** strategies. However, our understanding of where edges occur—and how they change  
**36** over time—remains limited, particularly at the boundaries of protected areas.

**37** Outside protected area borders, processes such as human settlement, land conver-  
**38** sion, or resource extraction can fragment landscapes and disrupt ecological continuity.

**39** Within protected areas, management interventions like prescribed burns or ecological  
**40** restoration can create edges. Together, these processes may lead to the ‘islandization’  
**41** of protected areas—where protected areas become functionally disconnected from the  
**42** broader land system despite their formal designation. Most analyses of edge dynamics  
**43** around protected areas focus on identifying edges along a single land cover type (e.g.,  
**44** forests) or are limited in geographic or temporal scale. Biome-wide assessments that  
**45** systematically quantify changes in edge presence or intensity over time remain rare.

**46** Here, we quantified the rate of change in edges along XXXX protected area bound-  
**47** aries across the world’s biomes for a 23-year period (2001–2023). We conducted a  
**48** comparative global assessment using 500 m MODIS satellite imagery and a pixel-  
**49** based approach to measure gradient magnitude across multiple spectral bands and  
**50** remote sensing indices. Gradient magnitude represents the intensity of spectral value  
**51** differences among neighboring pixels within a  $3 \times 3$  kernel, with higher values indicat-  
**52** ing greater local heterogeneity. To standardize edge detection, we computed an ‘edge  
**53** index’ for each protected area as the ratio of the median gradient magnitude of a 1  
**54** km diameter buffer to that of a 10 km diameter buffer, for all protected areas larger  
**55** than  $200 \text{ km}^2$  ( $n = XXXX$ ). By tracking changes in the edge index over time, our

56 approach isolated active edge dynamics from static landscape features (e.g., mountain  
57 ranges, elevation zones), offering new insight into the pace and extent of islandization  
58 across the world's protected landscapes.

## 59 **2 Methods**

60 We conducted a global assessment of edge dynamics in terrestrial protected areas  
61 using 500 m MODIS satellite imagery and a pixel-based approach to quantify spatial  
62 heterogeneity across protected area boundaries. Specifically, we calculated the gradient  
63 magnitude, a measure of spectral contrast among neighboring pixels, for multiple  
64 spectral bands and remote sensing indices. Gradient magnitude was computed within  
65 a  $3 \times 3$  kernel using:

$$66 \quad \text{Magnitude} = \sqrt{(\nabla_x I)^2 + (\nabla_y I)^2} \quad (1)$$

67 Higher gradient values indicated greater local heterogeneity. Because abrupt tran-  
68 sitions in land cover or land use create contrast in spectral values—"the gradient of  
69 [a] characteristic is steeper in the boundary than in either of the neighboring patches"  
70 [8]. Using this logic, when a protected area boundary aligns with an edge, we expect  
71 higher gradient magnitude on the boundary than in a larger reference area. Thus, to  
72 detect edges at protected area boundaries, we defined an 'edge index' for each pro-  
73 tected area as the ratio of the median gradient magnitude within a 1 km buffer to  
74 that within a concentric 10 km buffer.

$$75 \quad \text{Edge Index} = \frac{\bar{X}_{\text{boundary}}}{\bar{X}_{\text{buffer}}} \quad (2)$$

### 76 **2.1 Protected Area Data**

77 Protected area geometries were obtained from the June 2021 release of the World  
78 Database on Protected Areas (WDPA) [1]. Consistent with prior global studies [2],

79 we excluded marine protected areas, protected areas lacking reported area or detailed  
80 geometry (i.e., points only), and those designated as “UNESCO-MAB Biosphere  
81 Reserves.” Only terrestrial protected areas classified as “designated,” “established,”  
82 or “inscribed” were retained, following WDPA best practices.

83 We limited our analysis to protected areas larger than 200 km<sup>2</sup> to ensure compati-  
84 bility with the 500 m spatial resolution of MODIS data and to reduce the likelihood  
85 that a 10 km buffer would overlap itself in smaller areas. We also excluded protected  
86 areas in the upper quartile of the perimeter-to-area ratio to avoid long, narrow shapes  
87 where buffers might intersect within the same protected area. These filters resulted  
88 in XXXX protected areas for analysis, removing 225,353—primarily small protected  
89 areas in Europe—while reducing the total protected area analyzed by only 7.66%.

## 90 **2.2 Geometric Operations**

91 For each protected area, we generated concentric buffers of 1 km and 10 km diameter  
92 centered on the protected area boundary. The 1 km buffer captured fine-scale hetero-  
93 geneity aligned with the administrative boundary, while the 10 km buffer captured  
94 the background landscape variability. We selected these distances to balance spatial  
95 precision with ecological relevance: 1 km was deemed suitable for detecting land cover  
96 transitions at the administrative line while accounting for any slight spatial impreci-  
97 sion in the WDPA dataset [1] and 10 km reflects an arbitrary but reasonable distance  
98 for monitoring protected area isolation and ecological differences.

99 Since we were interested in terrestrial land surface dynamics, we excluded water  
100 features by removing buffered areas that overlapped with the maximum extent of  
101 surface water using the Global Surface Water dataset (1984–2021) [3]. For each year  
102 and each band/index, we calculated the median gradient magnitude within the 1 km  
103 and 10 km buffers and derived the edge index as their ratio.

104 To examine how edge dynamics varied by biome, we overlaid each protected  
105 area with the global terrestrial ecoregions map [4], and assigned each protected area  
106 the largest biome by area. We also extracted the mean human modification score  
107 from the global Human Modification dataset (gHM), which quantifies cumulative  
108 human impact at 1 km<sup>2</sup> resolution (CITE). These variables were ultimately used to  
109 analyze relationships between edge dynamics, ecological context, and anthropogenic  
110 modification.

### 111 **2.3 Satellite Imagery**

112 We used annual global composites from the MODIS/Terra Surface Reflectance 8-Day  
113 L3 product (MOD09A1) at 500 m resolution, spanning 2001 to 2023. For each year,  
114 we generated annual median composites of bands 1–4 and computed two spectral  
115 indices: the Normalized Difference Vegetation Index (NDVI) to represent vegetation  
116 greenness, and the Bare Soil Index (BSI) to reflect exposed soil. These bands and  
117 indices were selected to capture key land cover properties across biomes, including  
118 vegetation structure, soil exposure, and anthropogenic features.

$$119 \quad \text{NDVI} = \frac{\text{NIR} - \text{RED}}{\text{NIR} + \text{RED}} \quad (3)$$

$$120 \quad \text{BSI} = \frac{(\text{SWIR2} + \text{RED}) - (\text{NIR} + \text{BLUE})}{(\text{SWIR2} + \text{RED}) + (\text{NIR} + \text{BLUE})} \quad (4)$$

121 To validate the suitability of 500 m imagery, we visually compared MODIS-derived  
122 gradients from 2023 with those from 30 m Landsat-8 imagery (fig. S1). MODIS better  
123 captured broad-scale land cover transitions and was less sensitive to fine-scale spectral  
124 noise (e.g., individual trees, buildings, paddocks), while providing consistent coverage  
125 over the 23-year study period. Landsat data, by contrast, suffered from data gaps due  
126 to the ETM+ Scan Line Corrector failure [5]. For the spatial scale of this study, which  
127 focused on protected areas greater than 200 km<sup>2</sup>, MODIS was most appropriate,

<sup>128</sup> though finer-resolution imagery (e.g., Landsat 30-meter, Sentinel 10 – 60-meter, Planet  
<sup>129</sup> 0.5-meter) may be preferable for analyses that include small protected areas.

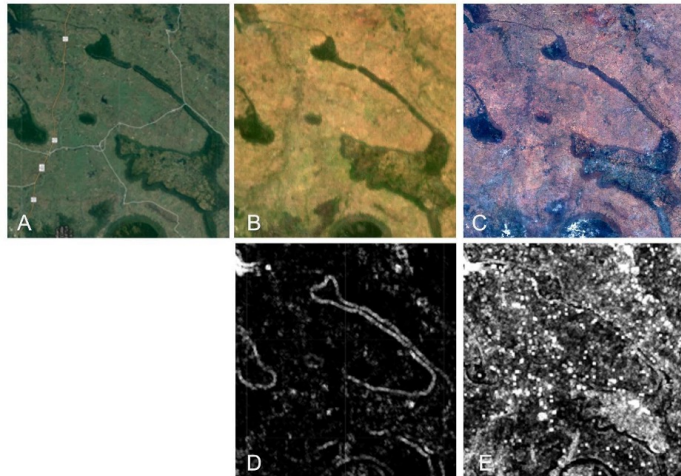


**Fig. 1 \***

Fig. S1. Original protected area satellite imagery and spectral gradient calculation of a protected area. (A) Google satellite image; (B) 2020 annual composite MODIS image (RGB band combination 1-4-3); (C) 2020 annual composite Landsat-8 image (RGB band combination 4-3-2); (D) gradient image calculated from MODIS (b), (E) gradient image calculated from Landsat-8 (C). As shown in (D), MODIS 500-meter pixel size was most adept at reducing fine-scale heterogeneity while retaining broad-scale patterns.

#### <sup>130</sup> **2.4 Statistical analyses**

<sup>131</sup> We used linear regression to estimate temporal trends in each protected area's edge  
<sup>132</sup> index from 2001 to 2023. Significance was determined using a threshold of  $p < 0.05$ ,  
<sup>133</sup> and we summarized the proportion of protected areas with significant trends by biome.  
<sup>134</sup> Because landscape change is not always linear, we also calculated a 10-year rolling  
<sup>135</sup> mean of the edge index to assess long-term dynamics. To quantify temporal variability,  
<sup>136</sup> we computed a 10-year rolling standard deviation. Additionally, we conducted break-  
<sup>137</sup> point analysis (CITE) to identify structural changes in edge dynamics and compared  
<sup>138</sup> the number of breakpoints across biomes.

139 To evaluate underlying environmental correlates of observed edge patterns, we  
140 calculated the annual rate of change in NDVI and BSI for each protected area and  
141 assessed correlations with 2021 gHM values.

142 Last, to assess the contemporary state of edge dynamics, we calculated the pro-  
143 portion of protected areas with an edge index greater than 1 in the year 2023. All  
144 spatial analyses were performed using the `geemap` Python package (CITE), and all  
145 statistical analyses were conducted in Python (CITE).

### 146 3 Results

### 147 4 Discussion

### 148 5 References

149 **Acknowledgments.** We thank M.W. Brunson, C.E. Aslan, W. Ji, I. Dronova, A.  
150 Merenlender, and A. Middleton for their comments on this study and manuscript.  
151 Special thanks to the Middleton and Brashares lab groups at UC Berkeley, and  
152 anonymous reviewers for helpful feedback and edits.

### 153 References

- 154 [1] Hanson, J. O. wdpar: Interface to the World Database on Protected Areas. *J.*  
155 *Open Source Softw.* **7**, 4594 (2022).
- 156 [2] Butchart, S. H. M. *et al.* Shortfalls and Solutions for Meeting National and Global  
157 Conservation Area Targets. *Conserv. Lett.* **8**, 329–337 (2015).
- 158 [3] Pekel, J.-F., Cottam, A., Gorelick, N. & Belward, A. S. High-resolution mapping  
159 of global surface water and its long-term changes. *Nature* **540**, 418–422 (2016).

- <sup>160</sup> [4] Dinerstein, E. *et al.* An Ecoregion-Based Approach to Protecting Half the  
<sup>161</sup> Terrestrial Realm. *Bioscience* **67**, 534–545 (2017).
- <sup>162</sup> [5] Arvidson, T., Goward, S., Gasch, J. & Williams, D. Landsat-7 long-term acquisi-  
<sup>163</sup> tion plan: Development and validation. *Photogramm. Eng. Remote Sens.* **72**, 1137  
<sup>164</sup> (2006).